Publisher's note: This SI document was uploaded to the platform on 14th April 2025, having been omitted in error.

Supporting Information

Optimizing Energy Level Alignment for Achieving Record-breaking Efficiency in Hot Exciton Deep Red OLEDs

Yujie Wu†, Jiasen Zhang†, Deli Li†, Songyu Du, Xilin Mu, Chunyu Liu, Kaibo Fang, Tingting Feng, Tao Wang, Wei Li,* and Ziyi Ge*

Y. J. Wu, J. S. Zhang, S. Y. Du, X. L. Mu, C. Y. Liu, K. B. Fang, T. T. Feng, Prof. W. Li, Prof. Z. Ge
Zhejiang Provincial Engineering Research Center of Energy Optoelectronic Materials and Devices, Ningbo Institute of Materials Technology and Engineering, Chinese Academy of Sciences, Ningbo, 315201, PR China
Center of Materials Science and Optoelectronics Engineering, University of Chinese Academy of Sciences, PR China
E-mail: liwei1987@nimte.ac.cn; geziyi@nimte.ac.cn
Y. J. Wu, T. Wang
School of Materials Science and Engineering
Zhejiang Sci-Tech University
Hangzhou 310018, P. R. China
Dr. D. L. Li
Institute for Smart Materials & Engineering, University of Jinan
No. 336 Nanxin Zhuang West Road, Jinan 250022, PR China

1. General Information

^{1}H and ^{13}C NMR spectra were recorded on a Bruker NMR spectrometer operating at 600 and 151 MHz, respectively. The mass spectrum was recorded by an AXIMA-CFRTM plus instrument and a JEOL JMS-K9 mass spectrometer. UV-vis spectra were recorded using Perkin-Elmer Lambda 950-PKA UV-Vis. All the low-temperature steady-state fluorescence and phosphorescence spectra were recorded by (Horiba Jobin Yvon) FluoroMax-4 Spectro-fluorometer with a Dewar flask. The low-temperature fluorescence spectra can be measured using stable-state fluorescence mode without time delay. The low-temperature phosphorescence can be recorded using phosphorescence mode after a time delay of 5 – 50 ms (delayed time adjusting range: 50 μs – 100 ms) to eliminate the influences of delayed fluorescence. Cyclic voltammetry measurement was conducted using the CHI-600D electro-chemical workstation. Photoluminescence quantum yields (PLQYs) in doped and non-doped films were measured utilizing an integrating sphere of Hamamatsu absolute PLQY spectrometer (C11347-01). Transient PL decay was evaluated with 280 nm and 340 nm LED excitation sources. Thermogravimetric analyses were conducted on a Netzsch TGA 2019F1 and Differential scanning calorimetry measurements were performed on a Netzsch DSC 214. Both TGA and DSC measurements were under N_2 flow.

1.1 Computational Methods

All the simulations were performed using the Gaussian 09_B01 program package.[1] For all the investigated molecules, the ground state (S_0) geometries were optimized using the M06-2X functional with a 6-31G* basis set in a vacuum for an initial guess. All the excited state was optimized by TD-DFT/M06-2X/6-31G* in toluene with a polarizable continuum model (PCM).[2]

1.2 Single-Crystal Analysis

According to the molecular exciton theory, the exciton splitting energy (Δε) in the case of dimer can be calculated: [3]

$$\Delta\varepsilon = \frac{2|M|^2}{r_{uv}^3}(cos\alpha - 3cos\theta_1 cos\theta_2) \quad (1)$$

,

where M is the electric dipole transition moment, α is the angle between the transition moments of the two molecules in the dimer, and θ_1 and θ_2 are the angles between transition moments of the two molecules and the interconnection of the centers. When $\Delta\varepsilon > 0$, it forms *H*-aggregation, when $\Delta\varepsilon < 0$, *J* type aggregation is formed.

1.3 Device Fabrication and Characterization

Glass substrates pre-coated with a 95-nm-thin layer of indium tin oxide (ITO) with a sheet resistance of 10 Ω per square was thoroughly cleaned in an ultrasonic bath of tetrahydrofuran, isopropyl alcohol, detergent, deionized water, and isopropyl alcohol and was then treated with O_2 plasma for 10 min in sequence. Organic layers were deposited onto the ITO-coated glass substrates by thermal evaporation under high vacuum (~10^{-5} Pa). The cathode was patterned using a shadow mask with an array of 3 mm × 3 mm openings. Deposition rates are 1 − 2 Å s^{-1} for organic materials and 2-5 Å s^{-1} for aluminum, respectively. Electroluminescence (EL) spectra were recorded by Photo Research PR745. The current density and luminance versus driving voltage characteristics EL spectra were measured by Keithley 2400 and Konica Minolta CS-2000 chromameter. EQEs were automatically calculated from the current density, luminance, and EL spectra, assuming a Lambertian distribution.

2. Synthesis

All reagents were purchased from the *Casmart Reagent Platform* and used as received without further purification. All compounds were synthesized via one-step common palladium-catalyzed Suzuki coupling reactions of ***8-bromo-5-(4-(tert-butyl)phenyl)-5H-pyrazino[2,3-b]indole-2,3-dicarbonitrile*** (**IPD-Br**) and corresponding boric acid-functionalized fragments. The synthetic routes of the key chemical intermediate IPD-Br can be referred to in our published work.[4]

Scheme S1. *The synthetic routes of* ***αT-IPD and βT-IPD***

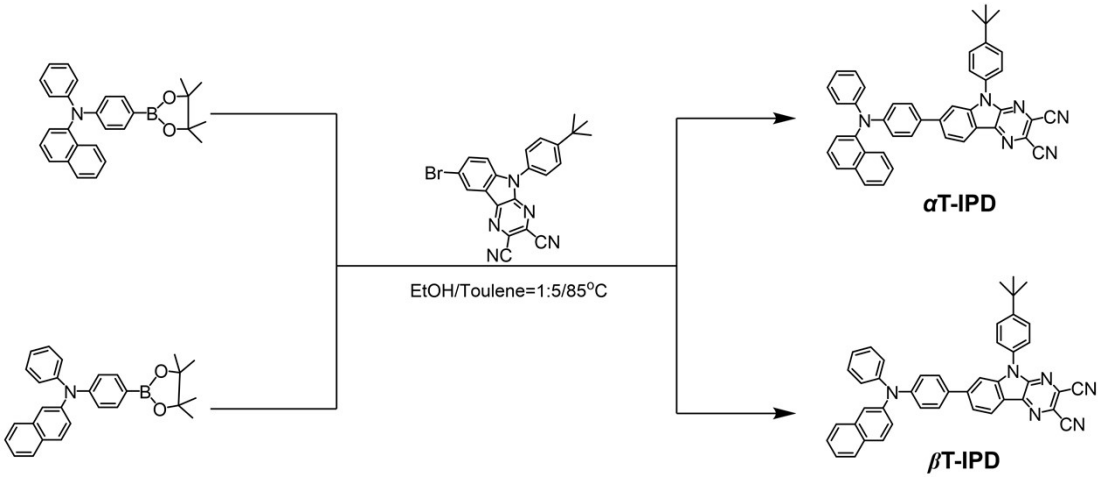

***Synthesis of target compound 5-(4-(tert-butyl)phenyl)-7-(4-(naphthalene-1-yl (phenyl)amino)phenyl)-5H-pyrazino[2,3-b]indole-2,3-dicarbonitrile (αT-IPD)*:** Compound **IPD-Br** (2 g, 4.65 mmol), *N-phenyl-N-(4-(4,4,5,5-tetramethyl-1,3,2-dioxaborolan-2-yl)phenyl) naphthalene-1-amine* (2.15 g, 5.11 mmol), $Pd(PPh_3)_4$ (0.48 g, 0.4 mmol), potassium carbonate (5.76 g, 40.16 mmol) were dissolved in 150 mL ultra-dry tetrahydrofuran into a 500 mL three-necked flask. The mixture was continuously stirred at 85° C for 12 hours under the nitrogen atmosphere. After cooling to room temperature, 200 mL of deionized water was added to the mixture. The reaction mixture was extracted with dichloromethane (3 x 100 mL), dried over anhydrous magnesium sulfate, and the solvent was removed under vacuum to give a red powder. The crude product was purified by column chromatography on silica gel (petroleum ether/dichloromethane = 2:3, v/v). The product was further purified by sublimation and obtained a 1.94 g dark red solid with a yield of 65%. ^{1}H NMR (400 MHz, Methylene Chloride-d_2) δ 8.48 (d, J = 8.4 Hz, 1H), 7.98 – 7.93 (m, 2H), 7.85 (d, J = 8.3 Hz, 1H), 7.80 (dd, J = 8.3, 1.5 Hz, 1H), 7.73 – 7.68 (m, 3H), 7.59 – 7.47 (m, 6H), 7.40 (ddd, J = 8.7, 7.2, 1.2 Hz, 2H), 7.27 (dd, J = 8.6, 7.2 Hz, 2H), 7.15 (dd, J = 8.6, 1.2 Hz, 2H), 7.07 – 7.01 (m, 3H), 1.44 (s, 9H). ^{13}C NMR (151 MHz, $CDCl_3$) δ 152.70, 149.30,

147.48, 146.41, 145.63, 144.27, 142.79, 138.69, 135.33, 131.83, 131.17, 130.42, 129.34, 128.56, 128.35, 127.45, 127.19, 127.17, 127.07, 126.67, 126.40, 126.35, 126.32, 125.05, 123.97, 123.76, 123.10, 123.04, 123.01, 120.61, 116.45, 114.77, 114.49, 108.86. ESI-TOF-MS ($C_{44}H_{32}N_6$): m/z: 645.2773 (M^++H), (M^+ calculated 644.2688).

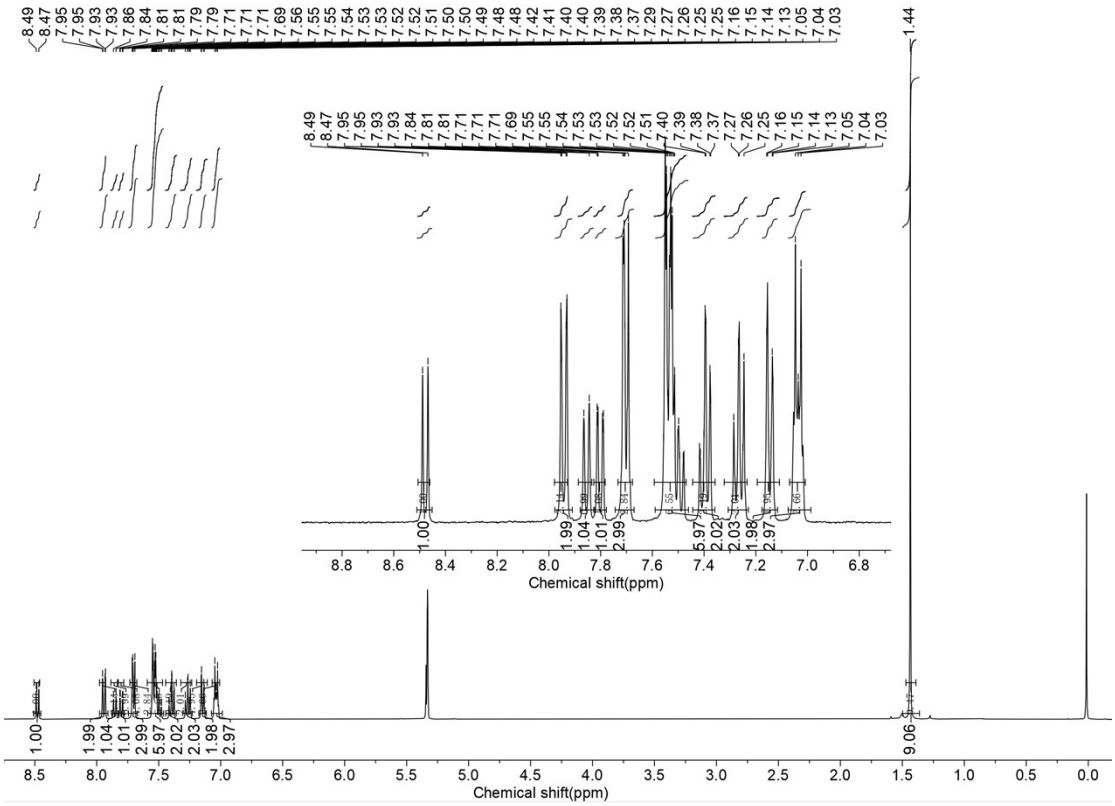

Figure S1. ^{1}H NMR spectrum of compound ***α*T-IPD**.

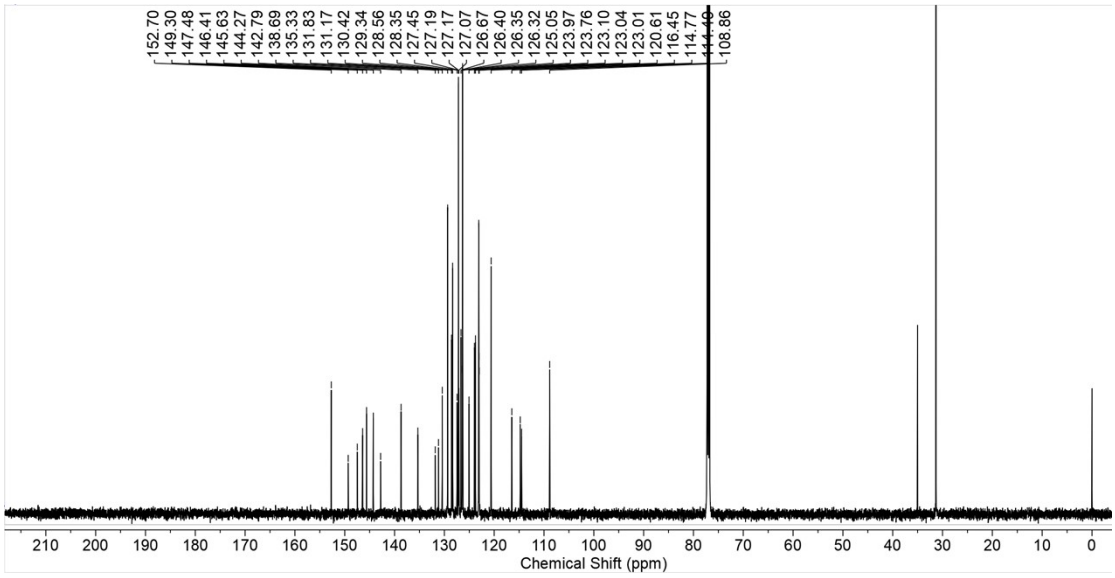

Figure S2. ^{13}C NMR spectrum of compound ***α*T-IPD**.

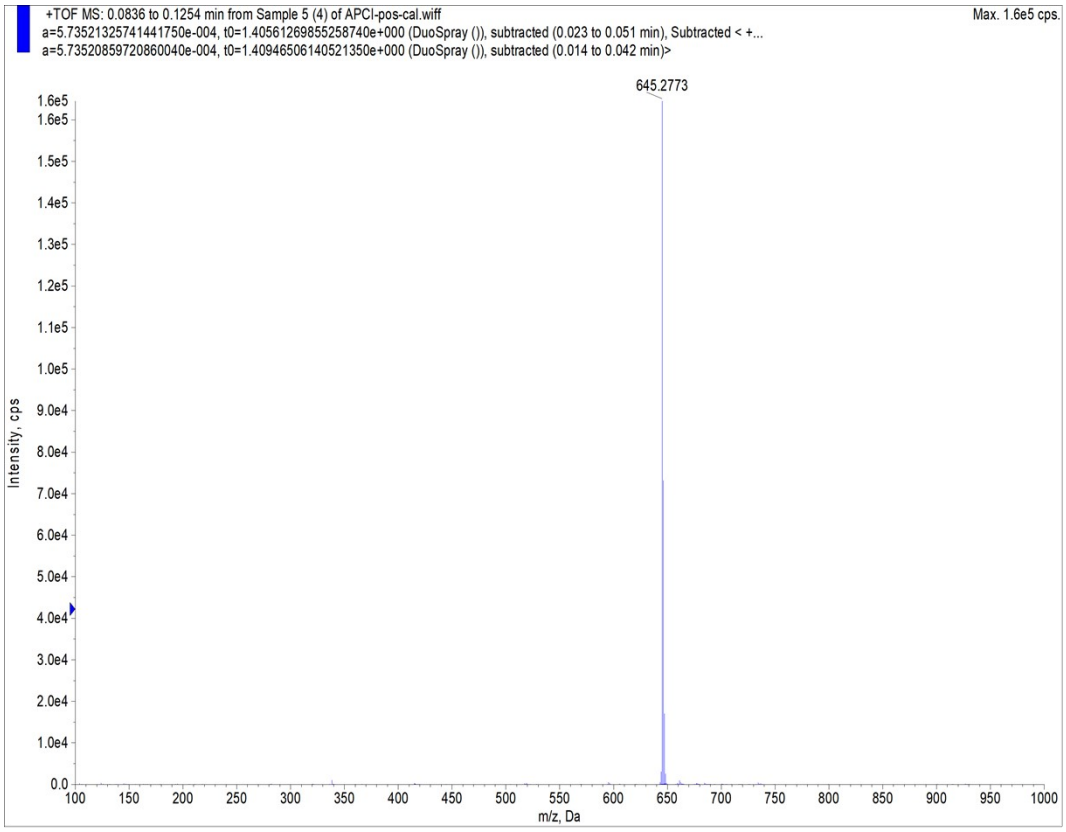

Figure S3. High-resolution mass spectrum of compound ***α*T-IPD**.

Synthesis of target compound 5-(4-(tert-butyl)phenyl)-7-(4-(naphthalene-2-yl (phenyl)amino)phenyl)-5H-pyrazino[2,3-b]indole-2,3-dicarbonitrile (βT-IPD)*:** Reaction of intermediate **IPD-Br** with ***N-phenyl-N-(4-(4,4,5,5-tetramethyl-1,3,2-dioxaborolan-2-yl)phenyl) naphthalene-2-amine following the same procedure for synthesis of ***α*T-IPD** generated the pure ***βT-IPD*** as a red powder. ^{1}H NMR (400 MHz, Methylene Chloride-d_2) δ 8.48 (d, J = 8.4 Hz, 1H), 8.00 – 7.92 (m, 2H), 7.85 (d, J = 8.3 Hz, 1H),

7.80 (dd, J = 8.3, 1.5 Hz, 1H), 7.74 – 7.68 (m, 3H), 7.58 – 7.49 (m, 6H), 7.40 (ddd, J = 8.7, 7.2, 1.2 Hz, 2H), 7.27 (dd, J = 8.6, 7.2 Hz, 2H), 7.20 – 7.12 (m, 2H), 7.08 – 6.98 (m, 3H), 1.44 (s, 9H). ^{13}C NMR (151 MHz, $CDCl_3$) δ 152.75, 148.68, 147.14, 146.25, 145.57, 144.74, 144.24, 138.59, 134.36, 133.11, 130.44, 130.41, 129.53, 129.19, 128.45, 127.62, 127.24, 127.20, 127.01, 126.45, 126.36, 125.15, 125.04, 124.97, 124.68, 123.89, 123.78, 123.20, 123.13, 121.49, 116.59, 114.73, 114.45, 109.05. ESI-TOF-MS ($C_{44}H_{32}N_6$): m/z: 645.2757 (M^++H), (M^+ calculated 644.2688).

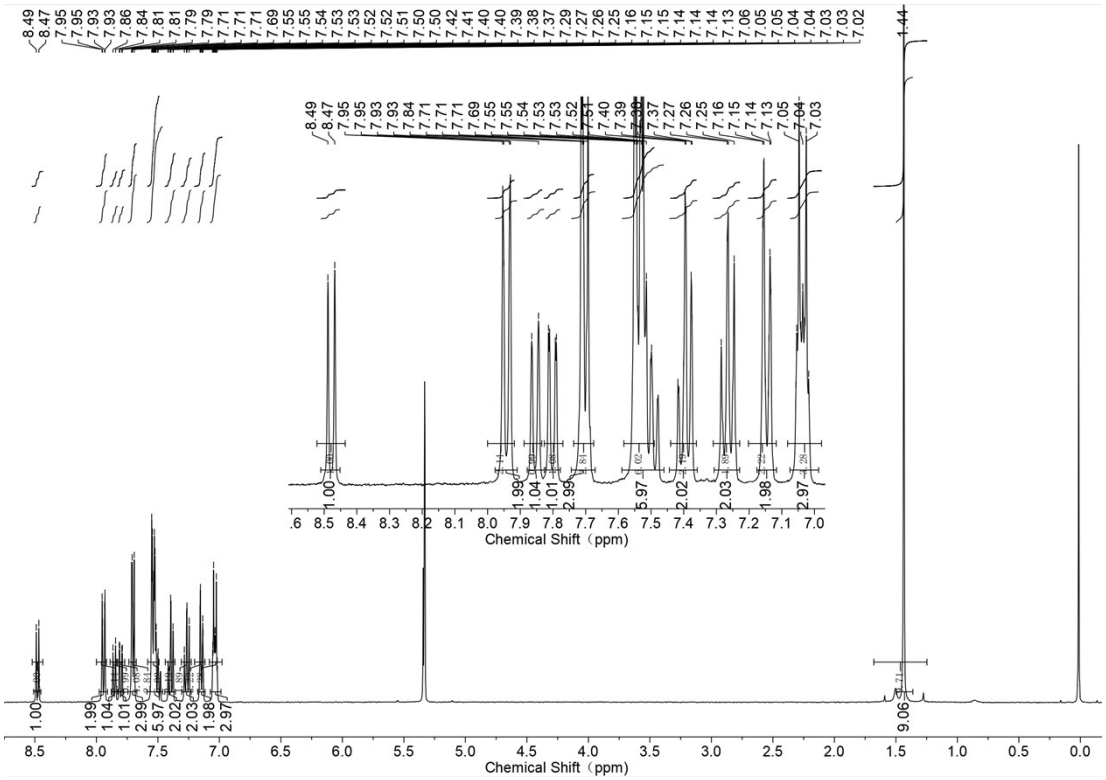

Figure S4. ^{1}H NMR spectrum of compound ***β*T-IPD**.

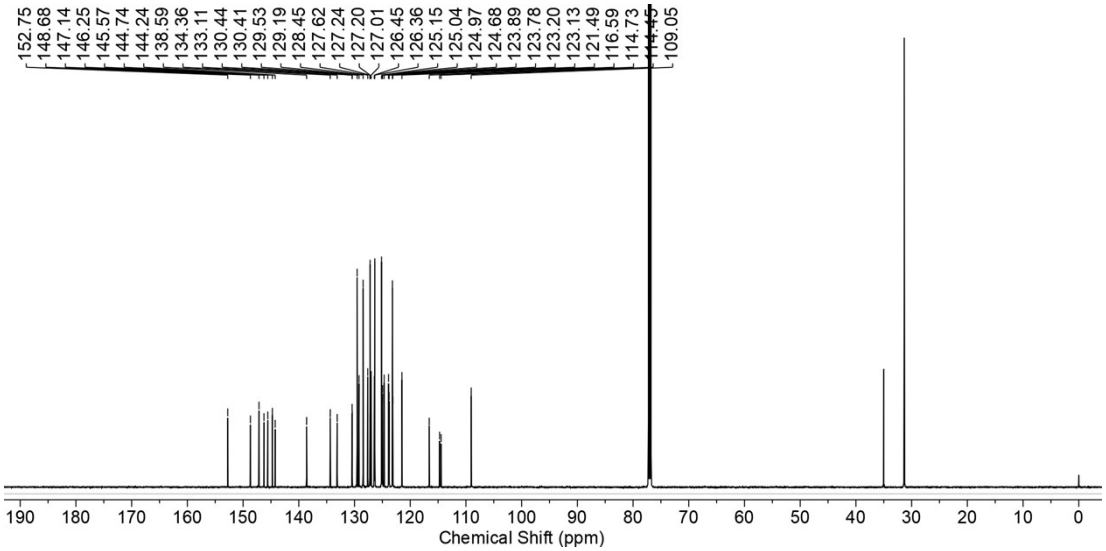

Figure S5. ^{13}C NMR spectrum of compound ***β*T-IPD**.

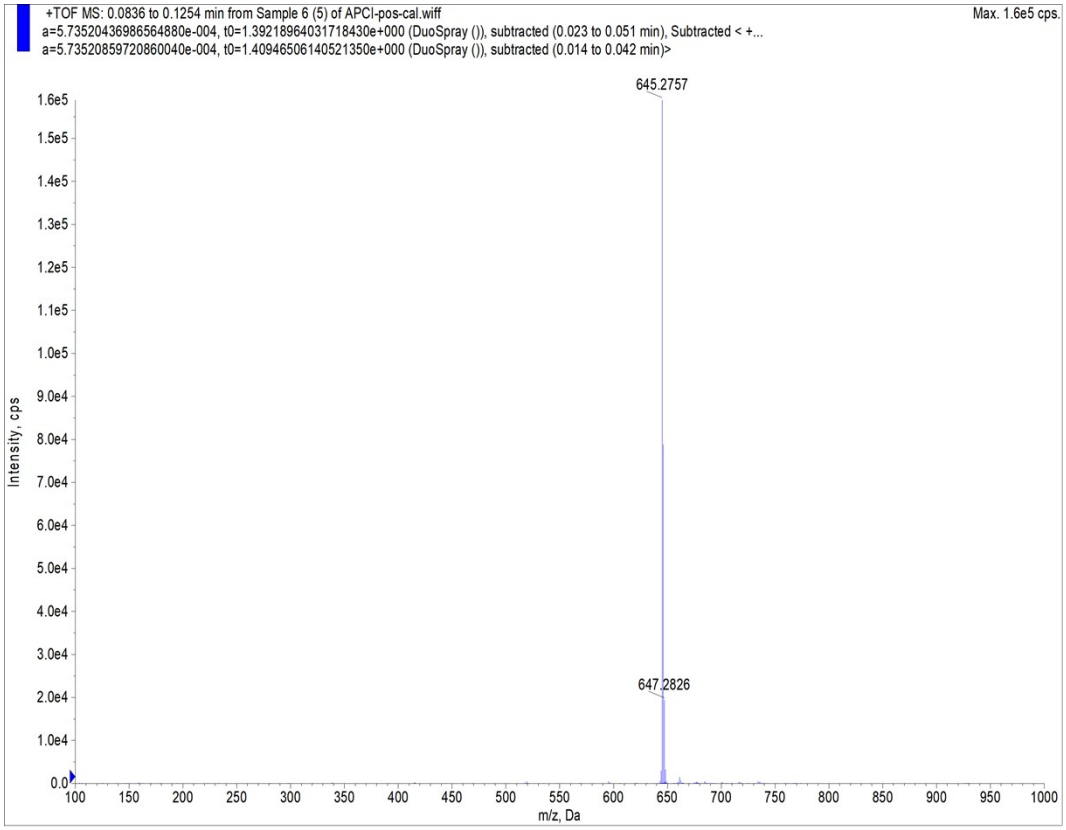

Figure S6. High-resolution mass spectrum of compound ***β*T-IPD**.

3. Thermal Properties

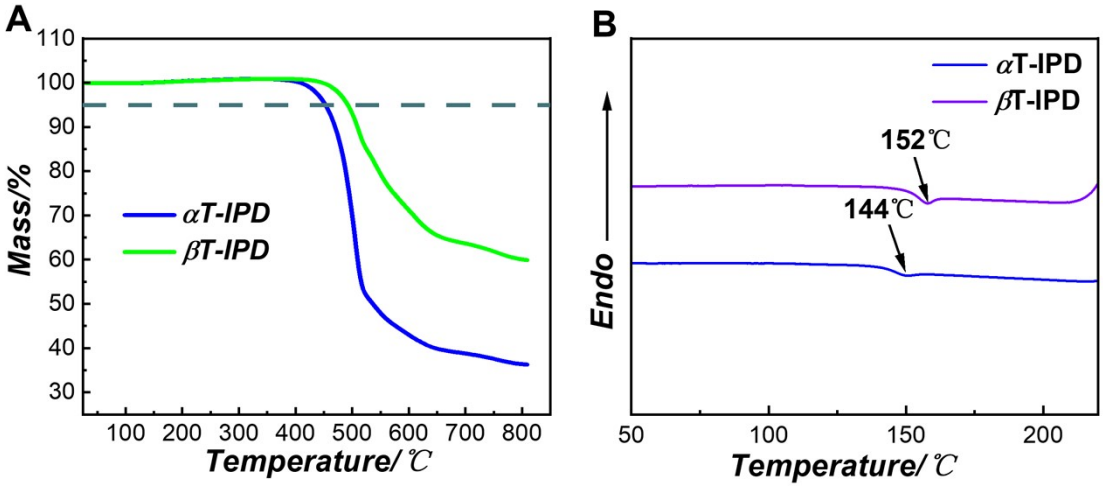

Figure S7. (a) thermogravimetric analysis and (b) differential scanning calorimetry measurements curses of T- αT-IPD and βT-IPD.

4. Computation

Mater.	S_1			T_1		
	Hole		Particle	Hole		Particle
αT-IPD	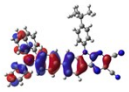	96.5% → f = 1.291	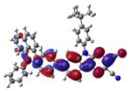	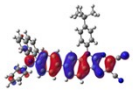	95.7% →	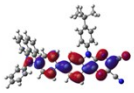
βT-IPD	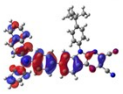	96.9% → f = 1.252	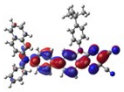	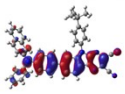	95.4% →	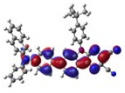

Figure S8. The natural transition orbitals (NTOs), oscillator strengths (*f*), and eigenvalues of the corresponding NTO pairs of *α*T-IPD and *β*T-IPD. All results were simulated based on the optimized S_1 and T_1 state geometries.

Mater.	T_1			T_2		
	Hole		Particle	Hole		Particle
αT-IPD	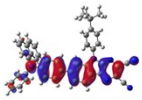	95.7% →	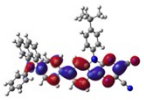	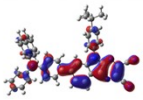	62.7% →	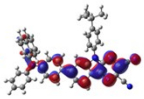
βT-IPD	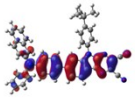	95.4% →	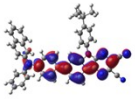	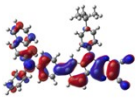	56.1% →	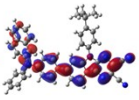

Figure S9. The NTOs and eigenvalues of the corresponding NTO pairs of *α*T-IPD and *β*T-IPD. All results were simulated based on the optimized T_1 state geometries.

5. Photo-Physical Properties

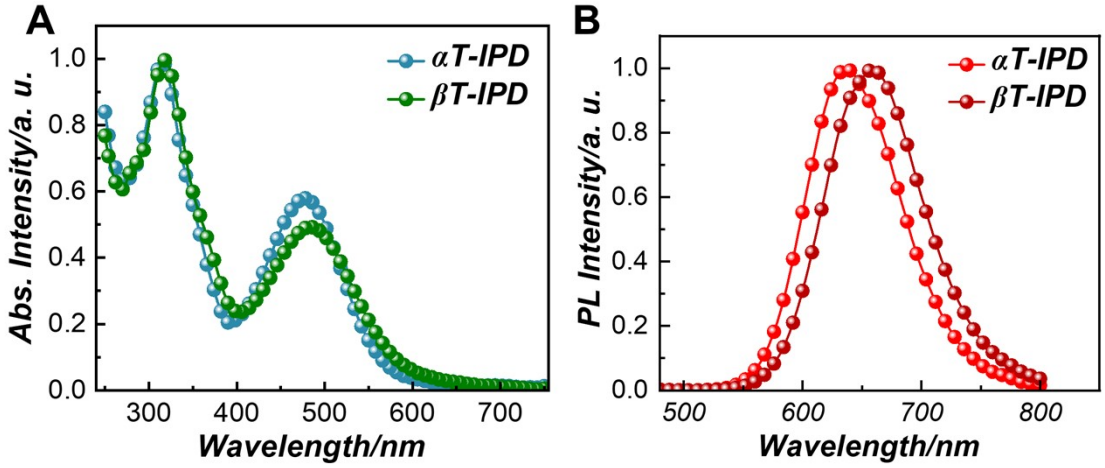

Figure S10. a) UV/vis absorption and b) PL spectra of αT-IPD and βT-IP in non-doped films.

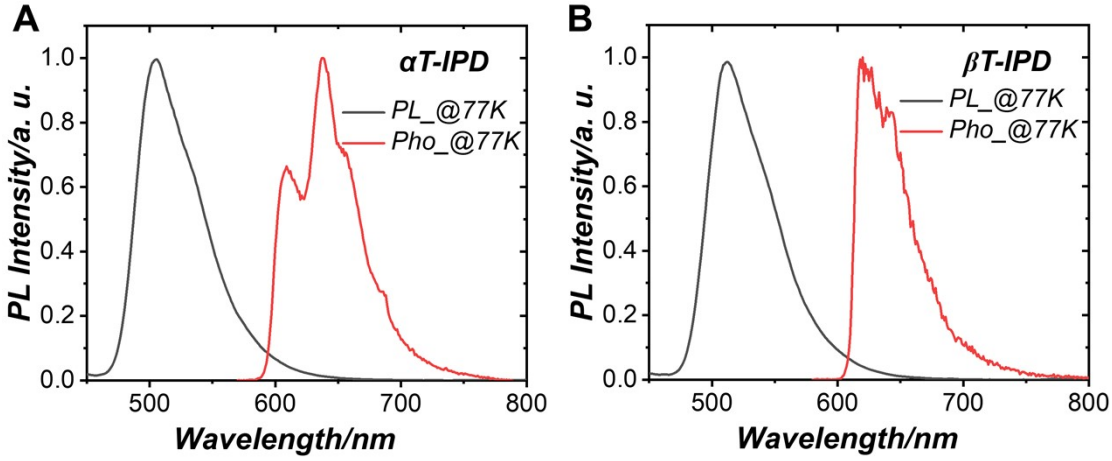

Figure S11. Low-temperature PL and phosphorescence spectra of a) αT-IPD and b) βT-IP dissolved in toluene solutions (0.01 mM). Conditions: PL at 77 K, phosphorescence at 77 K.

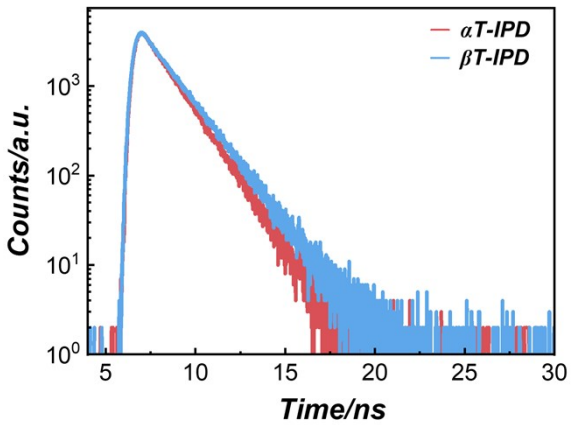

Figure S12. Transient PL decay spectra of αT-IPD and βT-IPD in non-doped films

6. Single crystal analysis

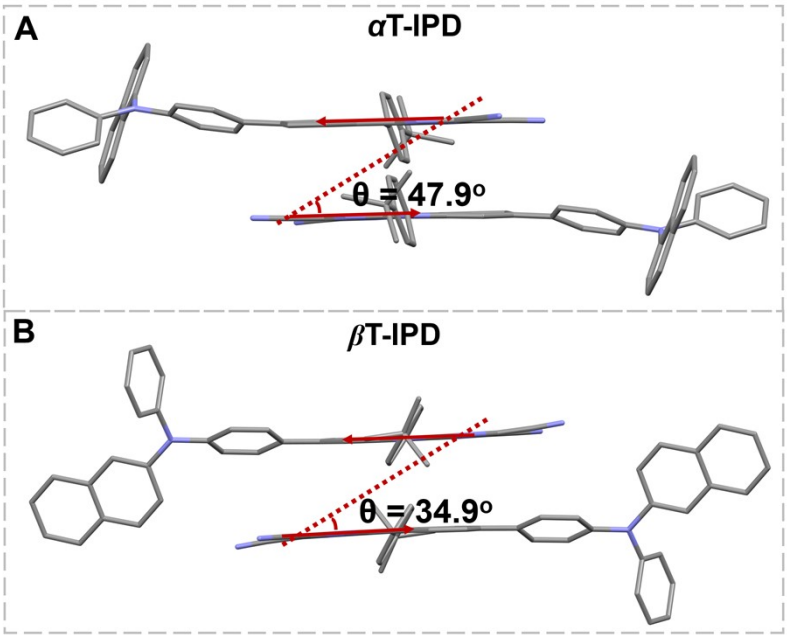

Figure S13. Packing motifs of aggregated dimers of (a) αT-IPD and (b) βT-IPD.

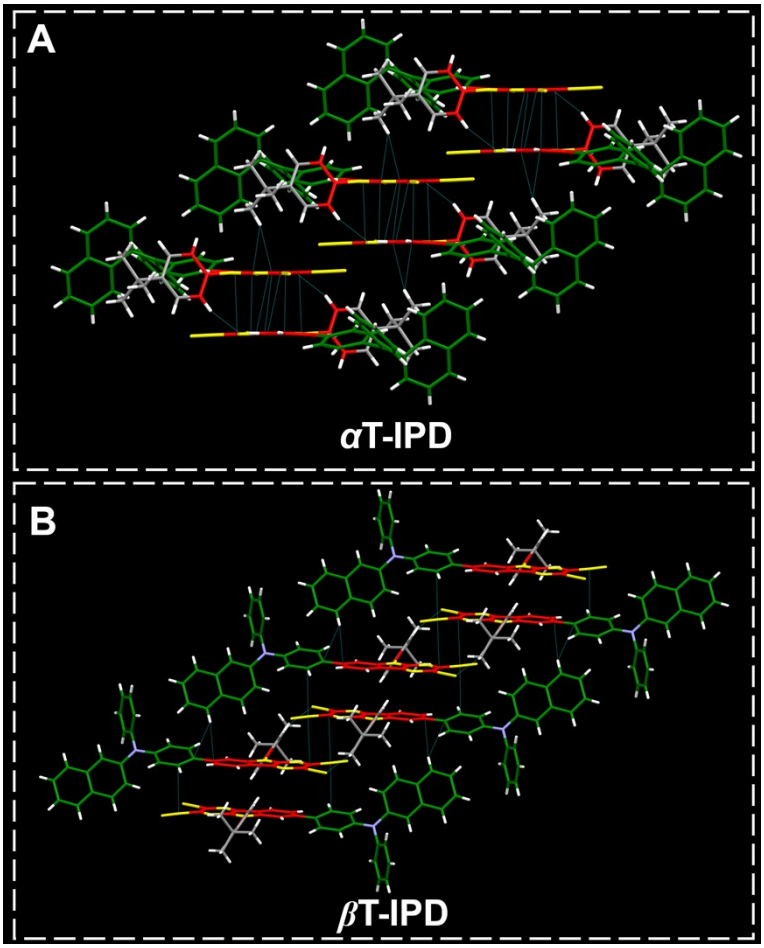

Figure S14. The molecular packing mode of (a) αT-IPD and (b) βT-IPD.

7. Energy Level

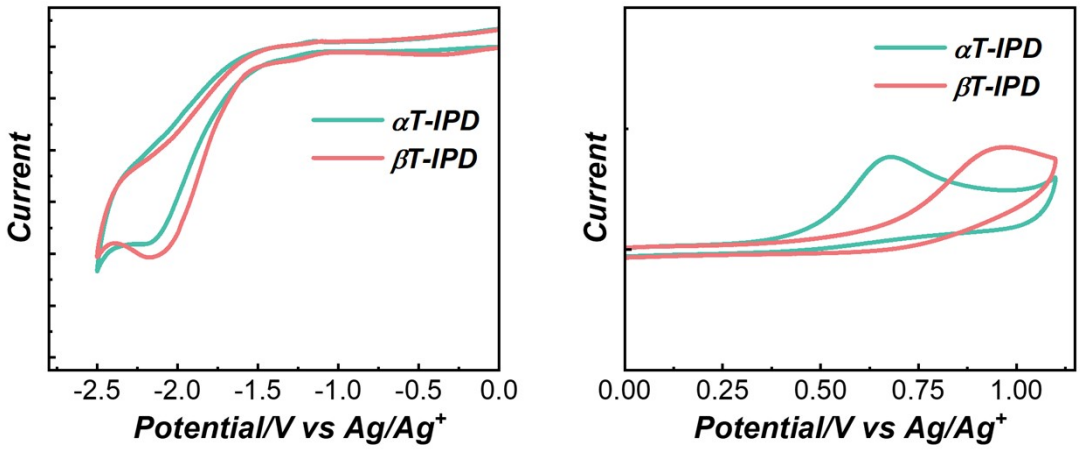

Figure S15. Cyclic voltammograms of αT-IPD and (b) βT-IPD in dichloromethane and acetonitrile mixed solvent (4:1) (anodic) and dimethylformamide (cathodic) at a scan rate of 100 mV s^{-1}.

8. Parameters of Photo-Physical Processes, Electrochemical and Thermal Stability and Single-Crystal

Table S1. Summary of photophysical properties of αT-IPD and βT-IPD.

	λ_{abs} [a)] [nm]	λ_{em} [a)] [nm]	ΔE_{ST} [b)] [eV]	ΔE_{ST} [c)] [eV]	Φ_{PLQY} [a)]	τ_p [a)] [ns]
αT-IPD	320/478	639	0.61	0.61	68.5	1.46
βT-IPD	320/484	660	0.61	0.61	73.5	1.64

[a)] Measured in the non-doped neat film; [b)] ΔE_{ST} evaluated in dilute toluene glass at 77K; [c)] calculated by TD-DFT simulation;

Table S2. Crystal data and structure refinement for αT-IPD and βT-IPD.

Identification code	αT-IPD	βT-IPD
Empirical formula	$C_{44}H_{32}N_6$	$C_{44}H_{32}N_6$
Formula weight /g mol^{-1}	644.75	644.75
Temperature /K	100K	100K
Crystal system	Monoclinic	Monoclinic
space group	P 2_1/n	C1 2/c 1
a (Å)	8.9279(4)	32.3110(13)
b (Å)	10.6851(4)	11.2344(5)
c (Å)	35.7149(14)	22.7693(9)
α (°)	90	90
β (°)	94.1710(10)	119.706(1)
γ (°)	90	90
Volume/ Å^3, Z	3398.02, 4	7178.93, 8
Density (CCDC)	1.260	1.19301
CCDC	2309641	2309564

Table S3. The electrochemical and thermal stability data of αT-IPD and βT-IPD.

Molecule	E_{HOMO} [d)] /(eV)	E_{LUMO} [d)] /(eV)	E_g /(eV)	T_d [a)] /(°C)	T_g /(°C)
αT-IPD	-4.9	-2.9	2.0	452	144
βT-IPD	-4.9	-2.9	2.0	459	152

[a)] Experimental HOMO/LUMO determined from cyclic voltammetry; [b)] Decomposition temperature (T_d) (5% weight loss).

9. Reference

[1] Frisch, M. J.; Trucks, G. W.; Schlegel, H. B.; Scuseria, G. E.; Robb, M. A.; Cheeseman, J. R.; Scalmani, G.; Barone, V.; Mennucci, B.; Petersson, G. A.; Nakatsuji, H.; Caricato, M.; Li, X.; Hratchian, H. P.; Izmaylov, A. F.; Bloino, J.; Zheng, G.; Sonnenberg, J. L.; Hada, M.; Ehara, M.; Toyota, K.; Fukuda, R.; Hasegawa, J.; Ishida, M.; Nakajima, T.; Honda, Y.; Kitao, O.; Nakai, H.; Vreven, T.; Montgomery, Jr., J. A.; Peralta, J. E.; Ogliaro, F.; Bearpark, M.; Heyd, J. J.; Brothers, E.; Kudin, K. N.; Staroverov, V. N.; Keith, T.; Kobayashi, R.; Normand, J.; Raghavachari, K.; Rendell, A.; Burant, J. C.; Iyengar, S. S.; Tomasi, J.; Cossi, M.; Rega, N.; Millam, J. M.; Klene, M.; Knox, J. E.; Cross, J. B.; Bakken, V.; Adamo, C.; Jaramillo, J.; Gomperts, R.; Stratmann, R. E.; Yazyev, O.; Austin, A. J.; Cammi, R.; Pomelli, C.; Ochterski, J. W.; Martin, R. L.; Morokuma, K.; Zakrzewski, V. G.; Voth, G. A.; Salvador, P.; Dannenberg, J. J.; Dapprich, S.; Daniels, A. D.; Farkas, O.; Foresman, J. B.; Ortiz, J. V.; Cioslowski, J.; Fox, D. J. *Gaussian 09, Revision B.01*; Gaussian, Inc.: Wallingford, CT, **2010**.

[2] a) E. Runge, E. K. U. Gross, *Phys. Rev. Lett.* **1984**, *52*, 997; b) M. A. L. Marques, E. K. U. Gross, *Annu. Rev. Phys. Chem.* **2004**, *55*, 427 – 455.

[3] Z. An, C. Zheng, Y. Tao, R. Chen, H. Shi, T. Chen, Z. Wang, H. Li, R. Deng, X. Liu, W. Huang, *Nat. Mater.* **2015**, *14*, 685-690.

[4] S. Du, M. Luo, D. Li, L. Lyu, W. Li, M. Zhao, Z. Wang, J. Zhang, D. Liu, Y. Li, S. J. Su, Z. Ge, *Adv. Mater.* **2023**, *35*, 2303304.